Hydrogenotrophic methanogens of the mammalian gut: functionally similar, thermodynamically different -A modelling approach

Rafael Munoz Tamayo, Milka Popova, Maxence Tillier, Diego Morgavi, Gérard Fonty, Nicole Morel-Desrosiers

Hydrogenotrophic methanogens of the mammalian gut: functionally similar, thermodynamically different - A modelling approach

Rafael Muñoz-Tamayo[1*,¶], Milka Popova[2,¶], Maxence Tillier[2], Diego P. Morgavi [2], Jean-Pierre Morel [3], Gérard Fonty [3], Nicole Morel-Desrosiers[3]

[1]UMR Modélisation Systémique Appliquée aux Ruminants, INRA, AgroParisTech, Université Paris-Saclay, 75005, Paris, France

[2]Institute National de la Recherche Agronomique, UMR1213 Herbivores, Clermont Université, VetAgro Sup, UMR Herbivores, Clermont-Ferrand, France

[3]Université Clermont Auvergne, CNRS, LMGE, F-63000 Clermont-Ferrand, France

Running title: Thermodynamic and kinetic modelling of gut methanogens

*** Correspondence:** Rafael Muñoz-Tamayo, UMR Modélisation Systémique Appliquée aux Ruminants, INRA, AgroParisTech, 16 Rue Claude Bernard, Paris, 75005, France. Tel: 00 33 144081759. E-mail : Rafael.Munoz-Tamayo@inra.fr

¶ These authors contributed equally to this work

Abstract

Methanogenic archaea occupy a functionally important niche in the gut microbial ecosystem of mammals. Our purpose was to quantitatively characterize the dynamics of methanogenesis by integrating microbiology, thermodynamics and mathematical modelling. For that, *in vitro* growth experiments were performed with pure cultures of key methanogens from the human and ruminant gut, namely *Methanobrevibacter smithii*, *Methanobrevibacter ruminantium* and *Methanobacterium formicium*. Microcalorimetric experiments were performed to quantify the methanogenesis heat flux. We constructed an energetic-based mathematical model of methanogenesis. Our model captured efficiently the dynamics of methanogenesis with concordance correlation coefficients of 0.94 for CO_2, 0.99 for H_2 and 0.97 for CH_4. Together, experimental data and model enabled us to quantify metabolism kinetics and energetic patterns that were specific and distinct for each species despite their use of analogous methane-producing pathways. Then, we tested *in silico* the interactions between these methanogens under an *in vivo* simulation scenario using a theoretical modelling exercise. *In silico* simulations suggest that the classical competitive exclusion principle is inapplicable to gut ecosystems and that kinetic information alone cannot explain gut ecological aspects such as microbial coexistence. We suggest that ecological models of gut ecosystems require the integration of microbial kinetics with nonlinear behaviours related to spatial and temporal variations taking place in mammalian guts. Our work provides novel information on the thermodynamics and dynamics of methanogens. This understanding will be useful to construct new gut models with enhanced prediction capabilities and could have practical applications for promoting gut health in mammals and mitigating ruminant methane emissions.

Introduction

Methanogenic archaea inhabit the gastro-intestinal tract of mammals where they have established syntrophic interactions within the microbial community (1–3) playing a critical role in the energy balance of the host (4,5). In the human gut microbiota, the implication of methanogens in host homeostasis or diseases is poorly studied, but of growing interest (6). *Methanobrevibacter smithii* (accounting for 94% of the methanogen population) and *Methanosphaera stadtmanae* are specifically recognized by the human innate immune system and contribute to the activation of the adaptive immune response (7). Decreased abundance of *M. smithii* was reported in inflammatory bowel disease patients (8), and it has been suggested that methanogens may contribute to obesity (9). In the rumen, the methanogens community is more diverse though still dominated by *Methanobrevibacter* spp., followed by *Methanomicrobium* spp., *Methanobacterium* spp. (10) and *Methanomassillicoccus* spp (11). However, the proportion of these taxa could vary largely, with *Methanomicrobium mobile* and *Methanobacterium formicium* being reported as major methanogens in grazing cattle (12). Though methanogens in the rumen are essential for the optimal functioning of the ecosystem (by providing final electron acceptors), the methane they produce is emitted by the host animal, contributing to global greenhouse gas (GHG) emissions. The livestock sector is responsible for 14.5% of the anthropogenic GHG emissions, of which enteric methane from ruminants contributes to more than 40% of total emissions (13). Methanogens can be separated in two groups based on the presence or absence of cytochromes, which are membrane-associated electron transfer proteins providing energetic advantages for microbial growth (14). However, in the gastrointestinal tract of mammals, the only methanogens with cytochromes are the *Methanosarcinales* which are minor members of the community (4,15). Major rumen methanogens (16) and the dominant human archaeon *M. smithii* (17), are hydrogenotrophic archaea without cytochrome. Cytochrome-lacking methanogens exhibit lower growth yields than archaea with cytochromes (14). However, this apparent energetic disadvantage has been counterbalanced by a greater adaptation to the environmental conditions prevailing in the gastrointestinal tract (15), and by the establishment of syntrophic interactions with feed fermenting

66 microbes. This syntrophic cooperation centred on hydrogen allows the anaerobic reactions of substrate
67 conversion to proceed close to the thermodynamic equilibrium (18,19) (that is with Gibbs free energy
68 change close to zero).

69 To our knowledge, the impact of thermodynamics on human gut metabolism has been poorly addressed
70 in existing mathematical models (20–23). For the rumen, thermodynamic principles have been
71 incorporated already into mathematical research frameworks because of their important role in feed
72 fermentation, (24–29). Despite these relevant efforts, much work remains to be conducted for attaining
73 a predictive thermodynamic-based model that allows for quantitative assessment of the impact of the
74 thermodynamics on fermentation dynamics. Theoretical frameworks have been developed to calculate
75 stoichiometric and energetic balances of microbial growth from the specification of the anabolic and
76 catabolic reactions of microbial metabolism (30,31), and advances have been done to link
77 thermodynamics to kinetics (32–34). These works constitute a solid basis for tackling the
78 thermodynamic modelling of gut metabolism. In this respect, new knowledge on the extent of
79 methanogenesis could help to improve existing gut models. Accordingly, our purpose was to
80 quantitatively characterize the dynamics of hydrogen utilization, methane production, growth and heat
81 flux of three hydrogenotrophic gut methanogens by integrating microbiology, thermodynamics, and
82 mathematical modelling. We investigated the rate and extent of methanogenesis by performing *in vitro*
83 experiments with three methanogenic species representing major human and ruminant genera: *M.*
84 *smithii, M. formicium* and *Methanobrevibacter ruminantium*. To interpret and get the most out of the
85 resulting data, a mathematical model with thermodynamic basis was developed to describe the
86 dynamics of the methanogenesis. Our findings allowed to quantify metabolism kinetics and energetic
87 patterns that were specific and distinct for each species despite their use of analogous methane-
88 producing pathways and their common belonging to the group of cytochrome-lacking methanogenic
89 archaea.

Material and Methods

In vitro growth experiments

Archaeal strains and growth media

Archaeal strains used in the study were *M. ruminantium* M1 (DSM 1093), *M. smithii* PS (type strain DSM 861), and *M. formicium* MF (type strain DSM 1535). The growth media was prepared as previously described (35) and composition is summarized in Table S1 of the Supplementary material.

Experimental design and measures

Starter cultures were grown until reaching optical density at 660 nm (OD_{660}) of 0.400 ± 0.030. Optical density was measured on a Jenway spectrophotometer (Bibby Scientific). Then, 0.6 ml were used to inoculate one experimental tube. Commercially prepared high purity H_2/CO_2 (80%/20%) gas mix was added to inoculated tubes by flushing for 1 min at 2.5 Pa. Mean initial OD_{660} and pressure values are summarized in Table S2 of the Supplementary material. Growth kinetics for each strain were followed over 72 h. The experiment was repeated twice. Each kinetics study started with 40 tubes inoculated at the same time. At a given time point (3 h, 5 h, 6.5 h, 24 h, 26 h, 30 h, 47h, 72 h post inoculation), two tubes with similar OD_{660} values were sampled. The tubes were used for measuring gas parameters: pressure was measured using a manometer and composition of the gas phase was analysed by gas chromatography on a Micro GC 3000A (Agilent Technologies, France). One of the tubes was centrifuged 10 min at 13 000 g. The microbial pellet was weighed and stored at -20°C in 2 ml screw-cap tubes containing 0.4 g of sterile zirconia beads (0.3 g of 1 mm and 0.1 g of 0.5 mm).

DNA extraction and qPCR quantification of 16S rRNA genes

One ml of lysis buffer (50mM NaCl, 50 mM TrisHCl pH 7.6, 50 mM EDTA, 5 % SDS) was added directly to the frozen microbial pellet before homogenizing for 2 × 30 s at 5100 tours/min in a Precellys bead-beater (Bertin Instruments). Samples were centrifuged for 3 min at 14 000 g and the liquid phase transferred to a new tube before adding 600 µl of phenol–chloroform–3-methyl-1-butanol (25:24:1) solution. After centrifugation at 14 000 g for 3 min, the aqueous phase was transferred to a fresh tube and 500 µl of chloroform were added. The chloroform-washing step was repeated twice with centrifugation at 14000 g for 3 min between steps. The final volume of the aqueous phase was measured and DNA precipitation was initiated by adding 70% of the volume of isopropanol 100% and 10% of the volume of sodium acetate 3M. Sedimentation at 14 000 g for 30 min was again performed and the resulting DNA pellet was washed with 500 µl of ethanol 70% and dissolved in 50µl of molecular biology quality water. The extraction yield was checked on a Nanodrop 1000 Spectrophotometer (Thermo Fisher Scientific, France) and extracts run on a FlashGel System (Lonza, Rockland, Inc) to check integrity.

Copies of 16S rRNA genes were quantified using a qPCR approach. Primers used are those of Ohene-Adjei et al (36) ; reaction assay and temperature cycles were as described previously (37) . Triplicate qPCR quantification was performed on 20 ng of extracted DNA. Amplifications were carried out using SYBR Premix Ex Taq (TaKaRa Bio Inc., Otsu, Japan) on a StepOne system (Applied Biosystems, Courtabeuf, France). Absolute quantification involved the use of standard curves that had been prepared with gDNA of *Methanobrevibacter ruminantium* DSM 1093. PCR efficiency was of 103%. Results were expressed as copy numbers per ng of extracted DNA per g of microbial pellet. *M. smithii* and *M. ruminantium* strains used in this study possess two copies of 16S rRNA genes in their genomes. The number of cells was computed by dividing 16S copy numbers by 2.

133

134 ## Microcalorimetry

135 Microcalorimetric experiments were performed to determine the heat flux pattern of each methanogen.
136 Metabolic activity and microbial growth were monitored by using isothermal calorimeters of the heat-
137 conduction type (A TAM III, TA Instruments, France) equipped with two multicalorimeters, each
138 holding six independent minicalorimeters, allowed continuous and simultaneous recording as a
139 function of time of the heat flux produced by 12 samples. The bath temperature was set at 39°C; its
140 long-term stability was better than ± $1x10^{-4}$°C over 24h. Each minicalorimeter was electrically
141 calibrated. The specific disposable 4 mL microcalorimetric glass ampoules capped with butyl rubber
142 stoppers and sealed with aluminium crimps were filled with 1.75 mL of Balch growth media and
143 overpressed with 2.5 Pa of H_2/CO_2 80%/20% gas mixture for 30 s. There was no significant difference
144 in pressure at the beginning of the study. They were sterilized by autoclave and stored at 39°C until the
145 beginning of the microcalorimetric measurements. Actively growing cultures of methanogens (OD_{660}
146 of 0.280±0.030 for *M. smithii*, 0.271±0.078 for *M. ruminantium* and 0.142±0.042 for *M. formicium)*
147 were stored at -20°C in order to diminish microbial activity before inoculation. Cultures were thawed
148 for 30 min at ambient temperature and inoculation was carried out by injecting 0.25 mL of the culture
149 through the septum of the overpressed microcalorimetric ampoules just before inserting them into the
150 minicalorimeters. Samples took about two hours to reach the bath temperature and yield a stable zero
151 baseline. Blank experiments were also carried out by inserting ampoules that were not inoculated and,
152 as expected, no heat flux was observed confirming the medium sterility. Each experiment was repeated
153 thrice.

154 The heat flux $\left(\frac{dQ}{dt}\right)$, also called thermal power output P, was measured for each methanogen and blank
155 samples with a precision ≥ 0.2 μW. The heat flux data of each sample were collected every 5 minutes

during more than 10 days. The total heat Q was obtained by integrating the overall heat flux time curve using the TAM Assistant Software and its integrating function (TA Instruments, France).

Classically, the heat flux-time curve for a growing culture starts like the S-shaped biomass curve (a lag phase followed by an exponential growth phase) but differs beyond the growth phase, the heat flux being then modulated by transition periods (38). Heat flux data can be used to infer the microbial growth rate constant provided the existence of a correlation between isothermal microcalorimetry data and microbiological data (e.g., cell counts) at early growth (39). During the exponential growth phase, microbial growth follows a first-order kinetics defined by the specific growth rate constant μ_c (h^{-1}). Analogously, the heat flux follows an exponential behaviour determined by the parameter μ_c as described by (38,39).

$$\frac{dQ}{dt} = \mu_c \cdot Q \quad (1)$$

The growth rate constant μ_c can be determined by fitting the exponential part of the heat flux-time curve using the fitting function of the TAM Assistant Software. In our case study, careful selection of the exponential phase of heat flux dynamics was performed to provide a reliable estimation of the maximum growth rate constant from calorimetric data.

Mathematical model development

Modelling *in vitro* methanogenesis

The process of *in vitro* methanogenesis is depicted in Figure 1. The H_2/CO_2 mixture in the gas phase diffuses to the liquid phase. The H_2 and CO_2 in the liquid phase are further utilized by the pure culture to produce CH_4. Methane in the liquid phase diffuses to the gas phase.

Model construction was inspired by our previous dynamic models of human gut (20) and rumen *in vitro* fermentation (40) followed by certain simplifications. The model considers the liquid-gas transfer of carbon dioxide. Due to the low solubility of hydrogen and methane (41), the concentration of these two gases in the liquid phase was not modelled. We assumed that the dynamics of concentrations in the gas phase are determined by kinetic rate of the methanogenesis. To incorporate thermodynamic information, instead of using the Monod equation in the original formulation, we used the kinetic rate function proposed by Desmond-Le Quéméner and Bouchez (33). The resulting model is described by the following ordinary differential equations

$$\frac{dx_{\mathrm{H_2}}}{dt} = \mu_{\max} \cdot \exp\left(-\frac{K_{\mathrm{S}} \cdot V_{\mathrm{g}}}{n_{\mathrm{g,H_2}}}\right) \cdot x_{\mathrm{H_2}} - k_{\mathrm{d}} \cdot x_{\mathrm{H_2}} \tag{2}$$

$$\frac{ds_{\mathrm{CO_2}}}{dt} = -\frac{-Y_{\mathrm{CO_2}} \cdot \mu_{\max}}{Y} \cdot \exp\left(-\frac{K_{\mathrm{S}} \cdot V_{\mathrm{g}}}{n_{\mathrm{g,H_2}}}\right) \cdot x_{\mathrm{H_2}} - k_{\mathrm{L}}\mathrm{a} \cdot \left(s_{\mathrm{CO_2}} - K_{\mathrm{H,CO_2}} \cdot R \cdot T \cdot n_{\mathrm{g,CO_2}}/V_{\mathrm{g}}\right) \tag{3}$$

$$\frac{dn_{\mathrm{g,H_2}}}{dt} = -\frac{\mu_{\max}}{Y} \cdot \exp\left(-\frac{K_{\mathrm{S}} \cdot V_{\mathrm{g}}}{n_{\mathrm{g,H_2}}}\right) \cdot V_{\mathrm{L}} \cdot x_{\mathrm{H_2}} \tag{4}$$

$$\frac{dn_{\mathrm{g,CO_2}}}{dt} = V_{\mathrm{L}} \cdot k_{\mathrm{L}}\mathrm{a} \cdot \left(s_{\mathrm{CO_2}} - K_{\mathrm{H,CO_2}} \cdot R \cdot T \cdot n_{\mathrm{g,CO_2}}/V_{\mathrm{g}}\right) \tag{5}$$

$$\frac{dn_{\mathrm{g,CH_4}}}{dt} = \frac{Y_{\mathrm{CH_4}} \cdot \mu_{\max}}{Y} \cdot \exp\left(-\frac{K_{\mathrm{S}} \cdot V_{\mathrm{g}}}{n_{\mathrm{g,H_2}}}\right) \cdot V_{\mathrm{L}} \cdot x_{\mathrm{H_2}} \tag{6}$$

where $s_{\mathrm{CO_2}}$ is the concentration (mol/L) of carbon dioxide in the liquid phase and $x_{\mathrm{H_2}}$ is the biomass concentration (mol/L) of hydrogenotrophic methanogens. The numbers of moles in the gas phase are represented by the variables $n_{\mathrm{g,H_2}}, n_{\mathrm{g,CO_2}}, n_{\mathrm{g,CH_4}}$. The gas phase volume $V_{\mathrm{g}} = 20$ mL and the liquid phase volume $V_{\mathrm{L}} = 6$ mL. Liquid-gas transfer for carbon dioxide is described by a non-equilibria transfer rate which is driven by the gradient of the concentration of the gases in the liquid and gas phase. The transfer rate is determined by the mass transfer coefficient $k_{\mathrm{L}}\mathrm{a}$ (h^{-1}) and the Henry's law coefficients $K_{\mathrm{H,CO_2}}$ (M/bar). R (bar·(M · K)$^{-1}$) is the ideal gas law constant and T is the temperature (K).

196 Microbial decay is represented by a first-order kinetic rate with k_d (h^{-1}) the death cell rate constant.
197 Microbial growth was represented by the rate function proposed by Desmond-Le Quéméner and
198 Bouchez (33) using hydrogen as the limiting reactant

199 $$\mu = \mu_{max} \cdot \exp\left(-\frac{K_s \cdot V_g}{n_{g,H_2}}\right) \quad (7)$$

200 where μ is the growth rate (h^{-1}), μ_{max} (h^{-1}) is the maximum specific growth rate constant and K_s(mol/L)
201 the affinity constant. Equation (7) is derived from energetic principles following Boltzmann statistics
202 and uses the concept of exergy (maximum work available for a microorganism during a chemical
203 transformation). The affinity constant has an energetic interpretation since it is defined as

204 $$K_s = \frac{E_M + E_{dis}}{v_{harv} \cdot E_{cat}} \quad (8)$$

205 where E_{dis} (kJ/mol) and E_M (kJ/mol) are the dissipated exergy and stored exergy during growth
206 respectively. E_{cat} (kJ/mol) is the catabolic exergy of one molecule of energy-limiting substrate, and
207 v_{harv} is the volume at which the microbe can harvest the chemical energy in the form of substrate
208 molecules (33). E_{cat} is the absolute value of the Gibbs energy of catabolism ($\Delta G_{r,c}$) when the reaction
209 is exergonic ($\Delta G_{r,c}$<0) or zero otherwise. The stored exergy E_M is calculated from a reaction (destock)
210 representing the situation where the microbe gets the energy by consuming its own biomass. E_M is the
211 absolute value of the Gibbs energy of biomass consuming reaction ($\Delta G_{r,destock}$) when the reaction is
212 exergonic ($\Delta G_{r,destock}$<0) or zero otherwise. Finally, the dissipated exergy E_{dis} is the opposite of the
213 Gibbs energy of the overall metabolic reaction, which is a linear combination of the catabolic and
214 destock reactions. This calculation follows the Gibbs energy dissipation detailed in Kleerebezem and
215 Van Loosdrecht (31).

216 In our model, the stoichiometry of methanogenesis is represented macroscopically by one catabolic
217 reaction (R_1) for methane production and one anabolic reaction (R_2) for microbial formation. We

assumed that ammonia is the only nitrogen source for microbial formation. The molecular formula of microbial biomass was assumed to be $C_5H_7O_2N$ (41).

R_1: $4\ H_2 + CO_2 \rightarrow CH_4 + 2\ H_2O$

R_2: $10\ H_2 + 5\ CO_2 + NH_3 \rightarrow C_5H_7O_2N + 8\ H_2O$

In the model, the stoichiometry of the reactions is taken into account *via* the parameters Y, Y_{CO_2}, Y_{CH_4}, which are the yield factors (mol/mol) of microbial biomass, CO_2 and CH_4. The microbial yield factor Y was extracted from literature. We assumed that *M. smithii* and *M. ruminantium* have the same yield (being both Methanobrevibacter). This yield factor was set to 0.006 mol biomass/mol H_2, using the methane-based molar growth yield of 2.8 g biomass/mol CH_4 estimated for *M. smithii* (42) and the equations (9) and (11). Similarly, the yield factor for *M. formicium* was set to 0.007 mol biomass/mol H_2 using the methane-based molar growth yield of 3.5 g biomass/mol CH_4 reported by Schauer and Ferry (43). The fraction of H_2 utilized for microbial growth (reaction R_2) is defined by the yield factor Y (mol of microbial biomass/mol of H_2). Now, let f be the fraction of H_2 used for the catabolic reaction R_1. Reaction R_2 tells us that for every 10 moles of H_2 used in R_2, we get 1 mol of microbial biomass. Hence, it follows that

$$Y = \frac{1}{10} \cdot (1 - f) \tag{9}$$

If Y is known, the fraction f can be computed from Equation (9).

The yield factors of CO_2 and CH_4 can be expressed as functions of the the fraction f:

$$Y_{CO_2} = \left(\frac{1}{4}\right) \cdot f + \left(\frac{5}{10}\right) \cdot (1 - f) \tag{10}$$

$$Y_{CH_4} = \left(\frac{1}{4}\right) \cdot f \tag{11}$$

The model has two physicochemical parameters ($k_{\mathrm{L}}\mathrm{a}, K_{\mathrm{H,CO_2}}$) and four biological parameters ($\mu_{\max}, K_{\mathrm{s}}, Y, k_{\mathrm{d}}$). The initial condition for $s_{\mathrm{CO_2}}$is unknown and was also included in the parameter vector for estimation. The Henry's law coefficients are known values calculated at 39°C using the equations provided by Batstone et al. (41). If the article is accepted, an implementation of the model in the Open Source software Scilab (https://www.scilab.org/) will be made available at Zenodo (https://doi.org/10.5281/zenodo.3271611).

Theoretical model to study interactions among methanogens

The experimental study of microbial interactions requires sophisticated *in vitro* systems under continuous operation such as the one developed by Haydock *et al*. (44). In our work, we explored by means of mathematical modelling how the methanogens can interact under *in vivo* conditions. For this theoretical study, we elaborated a toy model based on the previous model for *in vitro* methanogenesis. Let us consider the following simple model for representing the consumption of hydrogen by the methanogenic species i under an *in vivo* scenario of continuous flow

$$\frac{dx_{\mathrm{H_2},i}}{dt} = \mu_{\max,i} \cdot \exp\left(-\frac{K_{\mathrm{s},i} \cdot V_{\mathrm{g}}}{n_{\mathrm{g,H_2}}}\right) \cdot x_{\mathrm{H_2};i} - D_i \cdot x_{\mathrm{H_2},i} \quad (12)$$

$$\frac{dn_{\mathrm{g,H_2}}}{dt} = q_{\mathrm{H_2}} - \frac{\mu_{\max,i}}{Y_i} \cdot \exp\left(-\frac{K_{\mathrm{s},i} \cdot V_{\mathrm{g}}}{n_{\mathrm{g,H_2}}}\right) \cdot V_{\mathrm{L}} \cdot x_{\mathrm{H_2},i} - b \cdot n_{\mathrm{g,H_2}} \quad (13)$$

where $q_{\mathrm{H_2}}$(mol/h) is the flux of hydrogen produced from the fermentation of carbohydrates. The kinetic parameters are specific to the species i ($x_{\mathrm{H_2},i}$). The parameter D_i (h^{-1}) is the dilution rate of the methanogens and b (h^{-1}) is an output substrate rate constant. Extending the model to n species with a common yield factor Y, the dynamics of hydrogen is given by

$$\frac{dn_{\mathrm{g,H_2}}}{dt} = q_{\mathrm{H_2}} - \frac{V_{\mathrm{L}}}{Y}\sum_{i=1}^{n} \mu_{\max,i} \cdot \exp\left(-\frac{K_{\mathrm{s},i} \cdot V_{\mathrm{g}}}{n_{\mathrm{g,H_2}}}\right) \cdot x_{\mathrm{H_2},i} - b \cdot n_{\mathrm{g,H_2}} \quad (14)$$

where the sub index i indicates the species. In our case study, $n = 3$.

Parameter identification

Before tackling the numerical estimation of the model parameters, we addressed the question of whether it was theoretically possible to determine uniquely the model parameters given the available measurements from the experimental setup. This question is referred to as structural identifiability (45). Structural identifiability analysis is of particular relevance for model whose parameters are biologically meaningful, since knowing the actual value of the parameter is useful for providing biological insight on the system under study (46). Moreover, in our case, we are interested in finding accurate estimates that can be further used as priors in an extended model describing the *in vivo* system.

We used the freely available software DAISY (47) to assess the structural identifiability of our model. Physical parameters ($k_{\mathrm{L}}\mathrm{a}, K_{\mathrm{H,CO_2}}$) were set to be known. The model was found to be structurally globally identifiable. In practice, however, to facilitate the actual identification of parameters and reduce practical identifiability problems such as high correlation between the parameters (48), we fixed some model parameters to values reported in the literature. The transport coefficient $k_{\mathrm{L}}\mathrm{a}$, the Henry's law coefficient $K_{\mathrm{H,CO_2}}$, and the dead cell rate constant k_{d} were set to be known and were extracted from Batstone et al. (41). Therefore, only the parameters $\mu_{\max}, K_{\mathrm{s}}$ and initial condition of $s_{\mathrm{CO_2}}$ were set to be estimated. To capitalize on the calorimetric data, we further assumed that $\mu_{\max}$ was equal to the specific rate constant μ_{c} estimated from the heat flux-time curve. By this, only the affinity constant for each strain and the initial condition of $s_{\mathrm{CO_2}}$ were left to be estimated.

The parameter identification for each methanogen was performed with the IDEAS Matlab® toolbox (49), which is freely available at http://genome.jouy.inra.fr/logiciels/IDEAS. The measured variables

are the number of moles in the gas phase (H_2, CH_4, CO_2). The Lin's concordance correlation coefficient (CCC) (50) was computed to quantify the agreement between the observations and model predictions.

Results

Methanogens biomass

Archaea-specific primers targeting the 16S rRNA gene were used to enumerate microbial cells in each pure culture. Three hours post inoculation microbial numbers varied from 7.62×10^7 to 2.81×10^8 and reached 10^9 after 72 hours of incubation. Table S3 summarizes microbial numbers at different sampling times.

Calorimetric pattern of methanogens

Figure 2 displays a representative isothermal calorimetric curve for each methanogen. The three measured heat flux dynamics of each methanogen were found to follow similar energetic patterns. *M. smithii* and *M. formicium* exhibited a lag phase of a few hours, while *M. ruminantium* was already metabolically active when introduced into the minicalorimeter though several attempts were made to obtain a lag phase by changing storage conditions and thawing the culture just before inoculating the microcalorimetric ampoules. The pattern of heat flux for all tested methanogens is characterized by one predominant peak which was observed at different times for each methanogen. *M. smithii* exhibited a second metabolic event occurring at 60 h with an increase of heat flux. The same phenomenon was observed for *M. formicium* but at a lower intensity that started at 140 h. One possible explanation for this event is cell lysis (39). The process was considered completed when the heat flux ceased marking the end of the metabolic activity. It is noted that *M. formicium* produced a small peak at 14 h (Fig. 2). A similar peak, but of much smaller size, was observed on the other curves obtained with this methanogen. *M. smithii* also exhibits a small peak (occurrence of 3 out of 3) at 7.4 h shown in the inset

of Figure 2. For *M. ruminantium*, we do not know whether the small peak exists since the initial part of the curve is missing. This small peak translates in a metabolic activity that remains to be elucidated.

The total heat (Q_m) produced during the methanogenesis process that took place under the present experimental conditions was, on average, -5.5 ± 0.5 J for the three methanogens (for *M. ruminantium*, the missing initial part of the heat flux-time curve was approximately estimated by extrapolating the exponential fit). As we shall see below, this experimental value is consistent with the theoretically expected value.

Estimation of thermodynamic properties

We defined two macroscopic reactions to represent the catabolism (R1) and anabolism (R2) of the methanogenesis (see Modelling in vitro methanogenesis section). All thermodynamic properties result from the contribution of both catabolic and anabolic reactions. In the Supplementary Material, the calculations of total heat (Q_{m}), enthalpy (ΔH_{m}), Gibbs energy (ΔG_{m}) and entropy (ΔS_{m}) of the methanogenesis are detailed. The estimated overall heat produced during the methanogenesis process under our experimental conditions was in average $Q_{\mathrm{m}} = -5.66$ J. This heat results from the sum of the heat of the catabolic reaction (Q_{c}) and the heat of the anabolic reaction (Q_{a}). From the total heat of the methanogenesis, the anabolic reaction contributes to 7% of the metabolic heat for *M. smithii* and *M. ruminantium*. For *M. formicium*, the contribution of the anabolic reaction to the metabolic heat is 9%. It is also interesting to note that there is a very good agreement between the theoretical value calculated above and the overall heat experimentally determined by microcalorimetry (-5.5 ± 0.5 J).

Table 1 shows the thermodynamic properties per mole of biomass formed during methanogenesis of *M. ruminantium*, *M. smithii* and *M. formicium* on H_2/CO_2. These properties are compared with values found in the literature for other methanogens grown on different substrates.

Dynamic description of *in vitro* kinetics

The developed mathematical model was calibrated with the experimental data from *in vitro* growth experiments in Balch tubes. Table 2 shows the parameters of the dynamic kinetic model described in Equations 2-6. The reported value of $\mu_{\max}$ for each methanogen corresponds to the average value obtained from three heat flux-time curves. From Table 2, it is concluded that *M. smithii* exhibited the highest growth rate constant, followed by *M. ruminantium* and finally *M. formicium*. In terms of the affinity constant K_s, while *M. smithii* and *M. ruminantium* are of the same order, the affinity constant for *M. formicium* is lower in one order of magnitude.

Figure 3 displays the dynamics of the compounds in the methanogenesis for the three methanogens. Experimental data are compared against the model responses. Table 3 shows standard statistics for model evaluation. The model captures efficiently the overall dynamics of the methanogenesis. Hydrogen and methane are very well described by the model with concordance correlation coefficients (CCC) of 0.99 and 0.97 respectively. For carbon dioxide, CCC = 0.94.

Figure 4 displays the dynamics for the methanogens as measured by the 16S rRNA gene, as well as the dynamics of biomass as predicted for the model. As observed, the microbes follow a typical Monod-like trajectory.

Discussion

Our objective in this work was to quantitatively characterize the dynamics of hydrogen utilization, methane production, growth and heat flux of three hydrogenotrophic methanogens by integrating microbiology, thermodynamics and mathematical modelling. Our model developments were instrumental to quantify energetic and kinetic differences between the three methanogens studied, strengthening the potentiality of microcalorimetry as a tool for characterizing the metabolism of

347 microorganisms (51). This modelling work provides estimated parameters that can be used as prior
348 values for other modelling developments of gut microbiota.

349 Energetic and kinetic differences between methanogens

350 Methanogenesis appears as a simple reaction with a single limiting substrate (H_2). The
351 microcalorimetry approach we applied revealed that this simplicity is only apparent and that
352 hydrogenotrophic methanogens exhibit energetic and kinetic differences. Methanogenesis is indeed a
353 complex process that can be broken down in several stages. The dominant metabolic phase is
354 represented by one peak that occurs at different times. The magnitude of the peak differs between the
355 methanogens and also the slope of the heat flux trajectories. The return time of the heat flux to the zero
356 baseline was also different. The energetic difference is associated with kinetic differences that translate
357 into specific kinetic parameters, namely affinity constant (K_s) and maximum growth rate constant
358 (μ_{max}). Previously, energetic differences between methanogens have been ascribed to the presence or
359 absence of cytochromes (14). These differences are translated into different yield factors, H_2 thresholds,
360 and doubling times. The kinetic differences revealed in this study for three cytochrome-lacking
361 methanogens indicate that factors other than the presence of cytochromes might play a role in the
362 energetics of methanogenesis. Interestingly, calorimetric experiments showed that *M. ruminantium*
363 was metabolically active faster than the other methanogens, characteristic that could explain the
364 predominance of *M. ruminantium* in the rumen (52). Looking at the expression of the affinity constant
365 (Equation (8)), the differences between the affinity constants among the methanogens can be explained
366 by the differences between the by the harvest volume v_{harv} and the yield factors. Note that in the kinetic
367 function developed by Desmond-Le Quéméner and Bouchez (33), the maximum growth rate did not
368 have any dependency on the energetics of the reaction. Our experimental study revealed that μ_{max} is
369 species-specific and reflects the dynamics of the heat flux of the reaction at the exponential phase. This
370 finding suggests that a further extension of the kinetic model developed by Desmond-Le Quéméner

371 and Bouchez (33) should include the impact of energetics on μ_{max}. Since our study is limited to three
372 species, it is important to conduct further research on other methanogens to validate our findings.

373

374 ## Thermodynamic analysis

375 Regarding the energetic information for different methanogens summarized in Table 1, it is observed
376 that the thermodynamic behaviour of the three methanogens is analogous to that observed for
377 *Methanobacterium thermoautotrophicum* (53). The values reported in Table 1 show indeed that the
378 methanogenesis on H_2/CO_2 is characterized by large heat production. The growth is highly exothermic,
379 with a ΔH_m value that largely exceeds the values found when other energy substrates are used. The
380 enthalpy change ΔH_m, which is more negative than the Gibbs energy change ΔG_m, largely controls the
381 process. Growth on H_2/CO_2 is also characterized by a negative entropic contribution $T\Delta S_m$ which, at
382 first sight, may look surprising since entropy increases in most cases of anaerobic growth (54).
383 However, this can be understood if one remembers that $T\Delta S_m$ corresponds in fact to the balance
384 between the final state and the initial state of the process, that is

385 $$T\Delta S_{\mathrm{m}} = \frac{(1-10Y)}{4Y} T\Delta S_{\mathrm{c}} + T\Delta S_{\mathrm{a}} = \frac{(1-10Y)}{4Y} T(S_{final} - S_{initial})_{\mathrm{c}} + T(S_{final} - S_{initial})_{\mathrm{a}}$$

386 Methanogenesis on H_2/CO_2 is particular because the final state of its catabolic reaction (1 mol CH_4 +
387 2 mol H_2O) involves a smaller number of moles than the initial state (4 mol H_2 + 1 mol CO_2), which
388 results in a significant loss of entropy during the process. For spontaneous growth in such a case, the
389 ΔH_{m} must not only contribute to the driving force but must also compensate the growth-unfavourable
390 $T\Delta S_{\mathrm{m}}$, which means that ΔH_{m} must be much more negative than ΔG_{m} (55). For this reason,
391 methanogenesis on H_2/CO_2, which is accompanied by a considerable decrease of entropy and a large

392 production of heat, has been designed as an entropy-retarded process (53). More generally, von Stockar
393 and Liu (55) noticed that when the Gibbs energy of the metabolic process is resolved into its enthalpic
394 and entropic contributions, very different thermodynamic behaviours are observed depending on the
395 growth type. These thermodynamic behaviours are: aerobic respiration is clearly enthalpy-driven (ΔH_m
396 << 0 and $T\Delta S_m > 0$), whereas fermentative metabolism is mainly entropy-driven ($\Delta H_m < 0$ and $T\Delta S_m$
397 >> 0). Methanogenesis on H_2/CO_2 is enthalpy-driven but entropy-retarded ($\Delta H_m << 0$ and $T\Delta S_m < 0$) ,
398 whereas methanogenesis on acetate is entropy-driven but enthalpy-retarded ($\Delta H_m > 0$ and $T\Delta S_m >> 0$).
399 In the present case, the highly exothermic growth of *M. ruminantium, M. smithii* and *M. formicium* on
400 H_2/CO_2 is largely due to the considerable decrease of entropy during the process: in fact, 50% of the
401 heat produced here serves only to compensate the loss of entropy. A proportion of 80% was found for
402 *M. thermoautotrophicum* (53), which results from the fact that their $T\Delta S_m$ and ΔH_m values are,
403 respectively, 2.7 and 1.7 times larger than ours. This difference might be due to the differences in the
404 temperature of the studies , namely 39°C in our study vs 60°C in the study by Schill et al. (53).

405

406 **Do our results inform on ecological questions such as species coexistence?**

407 The competitive exclusion principle (56) states that coexistence cannot occur between species that
408 occupy the same niche (the same function). Only the most competitive species will survive. Recently,
409 by using thermodynamic principles, Großkopf & Soyer (34) demonstrated theoretically that species
410 utilizing the same substrate and producing different compounds can coexist by the action of
411 thermodynamic driving forces. Since in our study the three methanogens perform the same metabolic
412 reactions, the thermodynamic framework developed Großkopf & Soyer (34) predicts, as the original
413 exclusion principle (56), the survival of only one species. By incorporating thermodynamic control on
414 microbial growth kinetics, Lynch et al (57) showed theoretically that differentiation of ATP yields can

415 explain ecological differentiation of methanogens over a range of liquid turnover rates. This theoretical
416 work predicts that for a fixed liquid turnover rate, only one species survives. For the continuous culture
417 of microorganisms, it has been demonstrated that at the equilibrium (growth rate equals the dilution
418 rate) with constant dilution rates and substrate input rates, the species that has the lowest limiting
419 substrate concentration wins the competition. From Eq. (12), the number of moles of hydrogen of the
420 species $n^*_{\mathrm{g,H_2},i}$ at the steady state is

421 $$n^*_{\mathrm{g,H_2},i} = \frac{K_{\mathrm{s},i} \cdot V_{\mathrm{g}}}{\log\left(\mu_{\mathrm{max},i}/D_i\right)}$$

422

423 Using the model parameters of Table 2, we studied *in silico* three possible competition scenarios,
424 assuming a constant environment (constant dilution rate D). Two dilution rates were evaluated: D=
425 0.021 h^{-1} (retention time = 48 h) and D = 0.04 h^{-1} (retention time = 25 h). A retention time of 48 h
426 corresponds to values measured in small ruminants (58) and to humans as we used in our gut model
427 (20). For higher retention times, the results obtained for 48 h hold. For D= 0.021 h^{-1}, we obtained that
428 $n^*_{\mathrm{g,H_2,Ms}}$ = 0.32 mmol, $n^*_{\mathrm{g,H_2,Mr}}$ = 0.68 mmol, $n^*_{\mathrm{g,H_2,Mf}}$ = 0.28 mmol, where the subindex Ms, Mr, Mf
429 stand for *M. smithii*, *M. ruminantium* and *M.formicium*. From these results, it appears that under a
430 constant environment, *M. formicium* will win the competition. Since $n^*_{\mathrm{g,H_2,Ms}} < n^*_{\mathrm{g,H_2,Mr}}$, *M.*
431 *ruminantium* will be extinguished before *M. smithii*. For D = 0.04 h^{-1}, we obtained that $n^*_{\mathrm{g,H_2,Ms}}$ = 0.49
432 mmol, $n^*_{\mathrm{g,H_2,Mr}}$ = 1.42 mmol, $n^*_{\mathrm{g,H_2,Mf}}$ = 1.57 mmol, and thus *M. smithii* wins the competition. To win
433 the competition, *M. ruminantium* requires longer retention times than its competitors. Retention times
434 of digesta longer than 48 h are physiologically uncommon, thus the presence of *M. ruminantium* in the
435 gut ecosystem can be explained, for example, from known adhesion properties (both *M. ruminantium*
436 and *M. smithii* genes encode adhesin-like proteins (59,60). To illustrate these aspects, we built a
437 multiple-species model with the three methanogens using Eq. (12) and Eq. (14). The parameter b was

set to 0.5 h^{-1} and the hydrogen flux production q_{H_2} rate was set to 0.02 mol/min. Figure 5A displays the dynamics of the three methanogens for the first scenario (D= 0.021 h^{-1}). It is observed that at 50 d only *M. formicium* survives. This result, however, is not representative of what occurs in the rumen where the three methanogens coexist (5,61). It is intriguing that in our toy model it is *M. formicium* that wins the competition, bearing in mind that *M. ruminantium* and *M. smithii* are more abundant than *M. formicium* (5,52). Figure 5 shows that selective conditions favour the survival of one species. Similar results can be obtained for the human gut by including the effect of pH on microbial growth (23) and setting the gut pH to select one of the species. On the basis of the competitive exclusion principle, it is thus intriguing that having a very specialized function, methanogens are a diverse group that coexist. Gut ecosystems, therefore, exhibit the paradox of the plankton introduced by Hutchinson (1961) that presents the coexistence of species all competing for the same substrate in a relatively isotropic or unstructured environment (62) . In the case of the rumen, our modelling work suggests that in addition to kinetic and thermodynamic factors, other forces contribute to the ecological shaping of the methanogens community in the rumen favouring the microbial diversity. Indeed, methanogenic diversity in the rumen results from multiple factors that include pH sensitivity, the association with rumen fractions (fluid and particulate material), and the endosymbiosis with rumen protozoa (5,52). For the human gut, ecological factors enable methanogens to coexist to a competitive environment where hydrogenotrophic microbes (acetogens, methanogenic archaea and sulfate-reducing bacteria) utilize H_2 *via* different pathways (63–65). Both in the human gut and in the rumen, microbes grow in association with biofilms that form a polymer-based matrix that provides nutritional and hydraulic advantages for microbial growth and resistance to shear forces (20,66). Indeed, in our modelling work of human gut fermentation (20), we suggested that, from the different actions the mucus has on colonic fermentation, the mechanism of promoting conditions for microbial aggregation appears as the most relevant factor for attaining the high microbial density and the high level of fibre degradation

462 characteristic of the human gut. Altogether, these factors result in nonlinear behaviours, spatial and
463 temporal variations that promote coexistence and diversity, that, as discussed in dedicated literature on
464 microbial ecology (67–71), render the classical formulation of the competitive exclusion principle
465 (56,72) inapplicable to gut ecosystems.
466 Finally, mathematical modelling is expected to enhance our understanding of gut ecosystems (66,73).
467 It is then key that in addition to metabolic aspects, mathematical models of gut fermentation incorporate
468 the multiple aspects that shape microbial dynamics to provide accurate predictions and improve insight
469 on gut metabolism dynamics and its potential modulation. For ruminants, the development of precision
470 livestock technologies provides promising alternatives for integrating real-time data of key animal
471 phenotypes such as feeding behaviour with mathematical models for estimating methane emissions
472 (74) and rumen function indicators at large scale. These tools will be instrumental to support livestock
473 management decisions and guide timely interventions. Similarly, for humans, mathematical models
474 coupled with electronic technologies for online monitoring of gut function (75) might facilitate the
475 diagnosis and the design of personalized therapies for gastrointestinal diseases.

476 # Acknowledgements

477 We are grateful to Dominique Graviou (UMRH, Inra) for her skilled assistance on the *in vitro* growth
478 experiments and qPCR assays. We thank the Inra PHASE department and the Inra MEM
479 metaprogramme for financial support.

480

481 # Conflict of interest

482 No conflict.

References

1. Miller TL, Wolin MJ, Hongxue Z, Bryant MP. Characteristics of methanogens isolated from bovine rumen. Appl Environ Microbiol. 1986;51:201–2.

2. Dridi B, Fardeau ML, Ollivier B, Raoult D, Drancourt M. Methanomassiliicoccus luminyensis gen. nov., sp. nov., a methanogenic archaeon isolated from human faeces. Int J Syst Evol Microbiol. 2012;62:1902–7.

3. Paul K, Nonoh JO, Mikulski L, Brune A. "Methanoplasmatales," thermoplasmatales-related archaea in termite guts and other environments, are the seventh order of methanogens. Appl Environ Microbiol. 2012;78:8245–53.

4. Dridi B, Raoult D, Drancourt M. Archaea as emerging organisms in complex human microbiomes. Anaerobe. 2011;17:56–63.

5. Carberry CA, Waters SM, Kenny DA, Creevey CJ. Rumen methanogenic genotypes differ in abundance according to host residual feed intake phenotype and diet type. Appl Env Microbiol. 2014;80:586–94.

6. Borrel G, McCann A, Deane J, Neto MC, Lynch DB, Brugère JF, et al. Genomics and metagenomics of trimethylamine-utilizing Archaea in the human gut microbiome. ISME J. 2017;11:2059–74.

7. Bang C, Weidenbach K, Gutsmann T, Heine H, Schmitz RA. The intestinal archaea Methanosphaera stadtmanae and Methanobrevibacter smithii activate human dendritic cells. PLoS One. 2014;9:e99411.

8. Ghavami SB, Rostami E, Sephay AA, Shahrokh S, Balaii H, Aghdaei HA, et al. Alterations of

the human gut Methanobrevibacter smithii as a biomarker for inflammatory bowel diseases. Microb Pathog. 2018;117:285–9.

9. Mathur R, Barlow GM. Obesity and the microbiome. Vol. 9, Expert Review of Gastroenterology and Hepatology. 2015. p. 1087–99.

10. Hook SE, Wright A-DG, McBride BW. Methanogens: methane producers of the rumen and mitigation strategies. Archaea. 2010;945785.

11. Poulsen M, Schwab C, Jensen BB, Engberg RM, Spang A, Canibe N, et al. Methylotrophic methanogenic Thermoplasmata implicated in reduced methane emissions from bovine rumen. Nat Commun. 2013;4:1428.

12. Jarvis GN, Strömpl C, Burgess DM, Skillman LC, Moore ERB, Joblin KN. Isolation and identification of ruminal methanogens from grazing cattle. Curr Microbiol. 2000;40:327–32.

13. Gerber P, Steinfeld H, Henderson B, Mottet A, Opio C, Dijkman J, et al. Tackling Climate Change through Livestock. Food and Agriculture Organization. 2013.

14. Thauer RK, Kaster AK, Seedorf H, Buckel W, Hedderich R. Methanogenic archaea: Ecologically relevant differences in energy conservation. Nat Rev Microbiol. 2008;6:579–91.

15. Morgavi DP, Forano E, Martin C, Newbold CJ. Microbial ecosystem and methanogenesis in ruminants. Animal. 2010;4:1024–36.

16. Friedman N, Jami E, Mizrahi I. Compositional and functional dynamics of the bovine rumen methanogenic community across different developmental stages. Environ Microbiol. 2017;19:3365–73.

17. Hansen EE, Lozupone CA, Rey FE, Wu M, Guruge JL, Narra A, et al. Pan-genome of the dominant human gut-associated archaeon, Methanobrevibacter smithii, studied in twins. Proc Natl Acad Sci. 2011;108(Supplement_1):4599–606.

18. Jackson BE, McInerney MJ. Anaerobic microbial metabolism can proceed close to thermodynamic limits. Nature. 2002;415:454–6.

19. Gonzalez-Cabaleiro R, Lema JM, Rodriguez J, Kleerebezem R. Linking thermodynamics and kinetics to assess pathway reversibility in anaerobic bioprocesses. Energy Environ Sci. 2013;6:3780–9.

20. Muñoz-Tamayo R, Laroche B, Walter E, Doré J, Leclerc M. Mathematical modelling of carbohydrate degradation by human colonic microbiota. J Theor Biol. 2010;266:189–201.

21. Van Wey AS, Lovatt SJ, Roy NC, Shorten PR. Determination of potential metabolic pathways of human intestinal bacteria by modeling growth kinetics from cross-feeding dynamics. Food Res Int. 2016;88:207–16.

22. Shoaie S, Ghaffari P, Kovatcheva-Datchary P, Mardinoglu A, Sen P, Pujos-Guillot E, et al. Quantifying Diet-Induced Metabolic Changes of the Human Gut Microbiome. Cell Metab. 2015;22:320–31.

23. Kettle H, Louis P, Holtrop G, Duncan SH, Flint HJ. Modelling the emergent dynamics and major metabolites of the human colonic microbiota. Environ Microbiol. 2015;17:1615–30.

24. Janssen PH. Influence of hydrogen on rumen methane formation and fermentation balances through microbial growth kinetics and fermentation thermodynamics. Anim Feed Sci Technol. 2010;160:1–22.

545 25. Kohn R a, Boston RC. The Role of Thermodynamics in Controlling Rumen Metabolism.
546 Model Nutr Util Farm Anim. 2000;11–24.

547 26. Offner A, Sauvant D. Thermodynamic modeling of ruminal fermentations. 2006;55:343–65.

548 27. Ungerfeld EM. A theoretical comparison between two ruminal electron sinks. Front Microbiol.
549 2013;4.

550 28. Van Lingen HJ, Plugge CM, Fadel JG, Kebreab E, Bannink A, Dijkstra J. Thermodynamic
551 driving force of hydrogen on rumen microbial metabolism: A theoretical investigation. PLoS
552 One. 2016;11:e0161362.

553 29. Ghimire S, Gregorini P, Hanigan MD. Evaluation of predictions of volatile fatty acid
554 production rates by the Molly cow model. J Dairy Sci. 2014;97:354–62.

555 30. Heijnen JJ, Dijken JP. In search of a thermodynamic description of biomass yields for the
556 chemotrophic growth of microorgansims. Biotechnol Bioengeneering. 1992;39:833–52.

557 31. Kleerebezem R, Van Loosdrecht MCM. A Generalized Method for Thermodynamic State
558 Analysis of Environmental Systems. Crit Rev Environ Sci Technol. 2010;40:1–54.

559 32. Hoh CY, Cord-Ruwisch R. A practical kinetic model that considers endproduct inhibition in
560 anaerobic digestion processes by including the equilibrium constant. Biotechnol Bioeng.
561 1996;51:597–604.

562 33. Desmond-Le Quemener E, Bouchez T. A thermodynamic theory of microbial growth. Isme J.
563 2014;8:1747–51.

564 34. Großkopf T, Soyer OS. Microbial diversity arising from thermodynamic constraints. ISME J.

2016;10:2725–33.

35. Wolfe RS. Techniques for cultivating methanogens. Methods Enzymol. 2011;494:1–22.

36. Ohene-Adjei S, Teather RM, Ivan M, Forster RJ. Postinoculation protozoan establishment and association patterns of methanogenic archaea in the ovine rumen. Appl Environ Microbiol. 2007;73(14):4609–18.

37. Popova M, Martin C, Eugene M, Mialon MM, Doreau M, Morgavi DP. Effect of fibre- and starch-rich finishing diets on methanogenic Archaea diversity and activity in the rumen of feedlot bulls. Anim Feed Sci Technol. 2011;166–67:113–21.

38. Bricheux G, Bonnet JL, Bohatier J, Morel JP, Morel-Desrosiers N. Microcalorimetry: a powerful and original tool for tracking the toxicity of a xenobiotic on Tetrahymena pyriformis. Ecotoxicol Env Saf. 2013;98:88–94.

39. Braissant O, Bonkat G, Wirz D, Bachmann A. Microbial growth and isothermal microcalorimetry: Growth models and their application to microcalorimetric data. Thermochim Acta. 2013;555:64–71.

40. Muñoz-Tamayo R, Giger-Reverdin S, Sauvant D. Mechanistic modelling of in vitro fermentation and methane production by rumen microbiota. Anim Feed Sci Technol. 2016;220:1–21.

41. Batstone DJ, Keller J, Angelidaki I, Kalyuzhnyi S V, Pavlostathis SG, Rozzi A, et al. Anaerobic Digestion Model No.1 (ADM1). IWA Task Group for Mathematical Modelling of Anaerobic Digestion Processes. IWA Publishing, London; 2002.

42. Pavlostathis SG, Miller TL, Wolin MJ. Cellulose Fermentation by Continuous Cultures of

Ruminococcus-Albus and Methanobrevibacter-Smithii. Appl Microbiol Biotechnol. 1990;33(1):109–16.

43. Schauer NL, Ferry JG. Metabolism of formate in Methanobacterium formicicum. J Bacteriol. 1980;142:800–7.

44. Haydock AK, Porat I, Whitman WB, Leigh JA. Continuous culture of Methanococcus maripaludis under defined nutrient conditions. FEMS Microbiol Lett. 2004;

45. Walter E, Pronzato L. Identification of Parametric Models from Experimental Data. Springer, London; 1997.

46. Muñoz-Tamayo R, Puillet L, Daniel JB, Sauvant D, Martin O, Taghipoor M, et al. Review: To be or not to be an identifiable model. Is this a relevant question in animal science modelling? Animal. 2018;12:701–12.

47. Bellu G, Saccomani MP, Audoly S, D'Angio L. DAISY: A new software tool to test global identifiability of biological and physiological systems. Comput Methods Programs Biomed. 2007;88:52–61.

48. Vanrolleghem PA, Vandaele M, Dochain D. Practical identifiability of a biokinetic model of activated-sludge respiration. Water Res. 1995;29:2561–70.

49. Muñoz-Tamayo R, Laroche B, Leclerc M, Walter E. IDEAS: A parameter identification toolbox with symbolic analysis of uncertainty and its application to biological modelling. In: IFAC Proceedings Volumes. 2009. p. 1271–6.

50. Lin LI. A concordance correlation-coefficient to evaluate reproducibility. Biometrics. 1989;45:255–68.

607 51. Ruiz T, Bec A, Danger M, Koussoroplis A, Aguer J, Morel J, et al. A microcalorimetric
608 approach for investigating stoichiometric constraints on the standard metabolic rate of a small
609 invertebrate. Ecol Lett. 2018;21:1714–22.

610 52. Janssen PH, Kirs M. Structure of the archaeal community of the rumen. Appl Environ
611 Microbiol. 2008;74:3619–25.

612 53. Schill NA, Liu JS, von Stockar U. Thermodynamic analysis of growth of Methanobacterium
613 thermoautotrophicum. Biotechnol Bioeng. 1999;64:74–81.

614 54. von Stockar U, Larsson C, Marison IW. Calorimetry and energetic efficiencies in aerobic and
615 anaerobic microbial growth. Pure Appl Chem. 1993;65:1889–92.

616 55. Von Stockar U, Liu JS. Does microbial life always feed on negative entropy? Thermodynamic
617 analysis of microbial growth. Biochim Biophys Acta - Bioenerg. 1999;1412:191–211.

618 56. Hardin G. The competitive exclusion principle. Science (80-). 1960;131:1292–7.

619 57. Lynch TA, Wang Y, van Brunt B, Pacheco D, Janssen PH. Modelling thermodynamic
620 feedback on the metabolism of hydrogenotrophic methanogens. J Theor Biol. 2019;477:14–23.

621 58. Udén P, Rounsaville TR, Wiggans GR, Van Soest PJ. The measurement of liquid and solid
622 digesta retention in ruminants, equines and rabbits given timothy (Phleum pratense) hay. Br J
623 Nutr. 1982;48:329–339.

624 59. Ng F, Kittelmann S, Patchett ML, Attwood GT, Janssen PH, Rakonjac J, et al. An adhesin
625 from hydrogen-utilizing rumen methanogen Methanobrevibacter ruminantium M1 binds a
626 broad range of hydrogen-producing microorganisms. Env Microbiol. 2016;18:3010–21.

627 60. Samuel BS, Hansen EE, Manchester JK, Coutinho PM, Henrissat B, Fulton R, et al. Genomic

and metabolic adaptations of Methanobrevibacter smithii to the human gut. Proc Natl Acad Sci. 2007;104:10643–8.

61. Kelly WJ, Leahy SC, Li D, Perry R, Lambie SC, Attwood GT, et al. The complete genome sequence of the rumen methanogen Methanobacterium formicicum BRM9. Stand Genomic Sci. 2014;9:15.

62. Hutchinson GE. The paradox of the plankton. Am Nat. 1961;95:137–45.

63. Bernalier A, Lelait M, Rochet V, Grivet JP, Gibson GR, Durand M. Acetogenesis from H2 and CO2 by methane- and non-methane-producing human colonic bacterial communities. FEMS Microbiol Ecol. 1996;19:193–202.

64. Nava GM, Carbonero F, Croix JA, Greenberg E, Gaskins HR. Abundance and diversity of mucosa-associated hydrogenotrophic microbes in the healthy human colon. ISME J. 2012;6:57–70.

65. Flint HJ, Duncan SH, Scott KP. Interactions and competition within the microbial community of the human colon : links between diet and health. Environ Microbiol. 2007;9:1101–11.

66. Huws SA, Creevey CJ, Oyama LB, Mizrahi I, Denman SE, Popova M, et al. Addressing global ruminant agricultural challenges through understanding the rumen microbiome: past, present, and future. Front Microbiol. 2018;9:2161.

67. Pfeiffer T, Schuster S, Bonhoeffer S. Cooperation and competition in the evolution of ATP-producing Pathways. Science (80-). 2001;292:50–507.

68. Vandermeer J, Evans MA, Foster P, Höök T, Reiskind M, Wund M. Increased competition may promote species coexistence. Proc Natl Acad Sci. 2002;99:8731–6.

649 69. MacLean RC, Gudelj I. Resource competition and social conflict in experimental populations
650 of yeast. Nature. 2006;441:498–501.

651 70. Rapaport A, Dochain D, Harmand J. Long run coexistence in the chemostat with multiple
652 species. J Theor Biol. 2009;257:252–9.

653 71. Grognard F, Masci P, Benoît E, Bernard O. Competition between phytoplankton and bacteria:
654 exclusion and coexistence. J Math Biol. 2015;70:959–1006.

655 72. Hsu SB, Hubbell S, Waltman P. A mathematical theory for single-nutrient competition in
656 continuous cultures of micro-organisms. SIAM J Appl Math. 1977;32:366–83.

657 73. Widder S, Allen RJ, Pfeiffer T, Curtis TP, Wiuf C, Sloan WT, et al. Challenges in microbial
658 ecology: Building predictive understanding of community function and dynamics. ISME J.
659 2016;10:2557–68.

660 74. Muñoz-Tamayo R, Ramirez Agudelo JF, Dewhurst RJ, Miller G, Vernon T, Kettle H. A
661 parsimonious software sensor for estimating the individual dynamic pattern of methane
662 emissions from cattle. Animal. 2018;

663 75. Ou JZ, Yao CK, Rotbart A, Muir JG, Gibson PR, Kalantar-zadeh K. Human intestinal gas
664 measurement systems: In vitro fermentation and gas capsules. Trends Biotechnol.
665 2015;33:208–13.

666

667

668

669 **Figures**

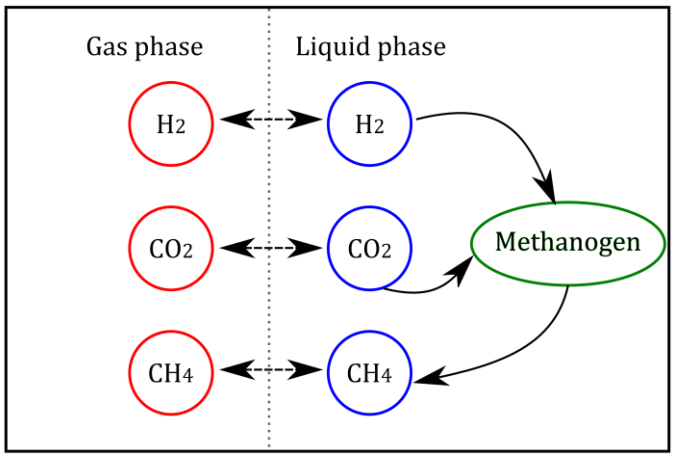

670

671 **Figure 1** Schematics of the *in vitro* methanogenesis process by hydrogenotrophic methanogens.

672 Double arrows represent fluxes due to liquid-gas transfer, simple arrows represent metabolic fluxes.

673

674

675

676

677

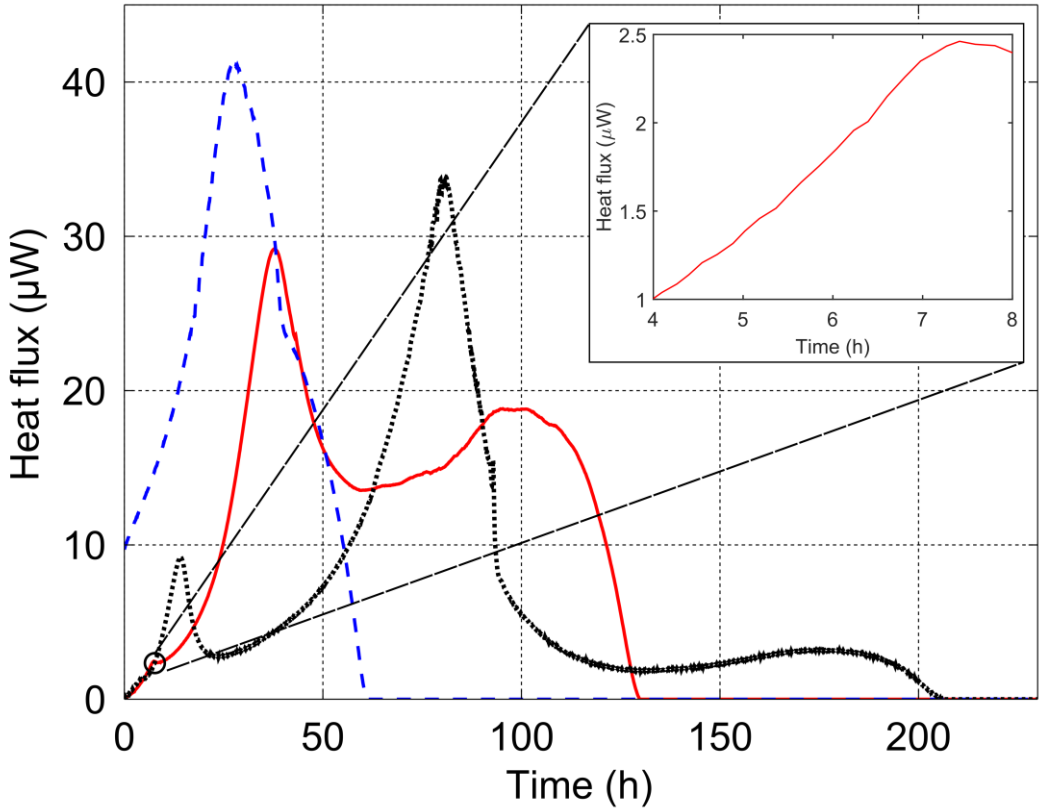

678

679 **Figure 2** Example of isothermal calorimetric curves for *M. ruminantium* (dashed blue line), *M. smithii*
680 (solid red line) and *M. formicium* (dotted black line). The dominant metabolic phase is represented by
681 one peak. The magnitude of the peak differs between the methanogens and also the slope of the heat
682 flux trajectories. The return of the heat flux to the zero baseline also differs between the three
683 methanogens. The inset zoom displays the peak exhibited by *M. smithii* at 7.4 h.

684

685

686

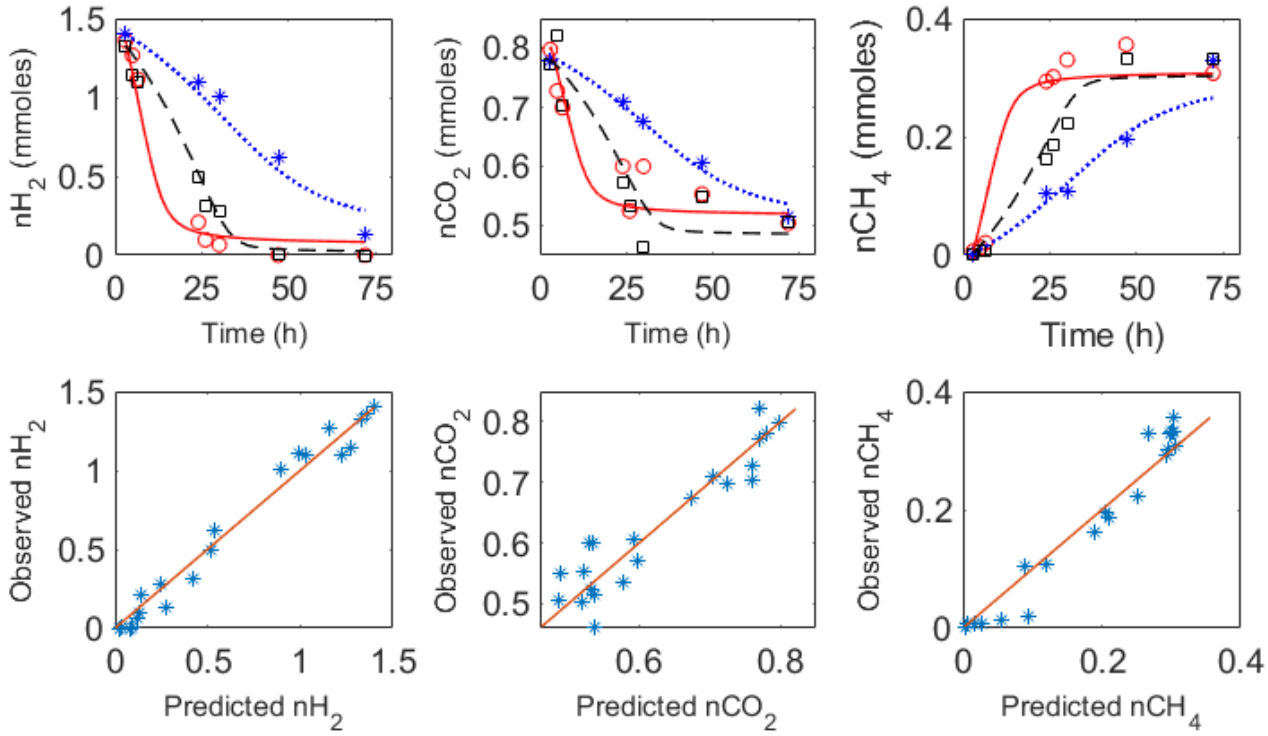

687

688 **Figure 3** Top plots: dynamics of methanogenesis by *M. ruminantium* (*), *M. smithii* (o) and *M.*

689 *formicium* (□). Experimental data (*,o,□) are compared against model predicted responses: dotted blue

690 lines (*M. ruminantium*), solid red lines (*M. smithii*) and dashed black lines (*M. formicium*). Bottom

691 plots: summary observed vs predicted variables**.** The solid red line is the isocline.

692

693

694

695

696

697

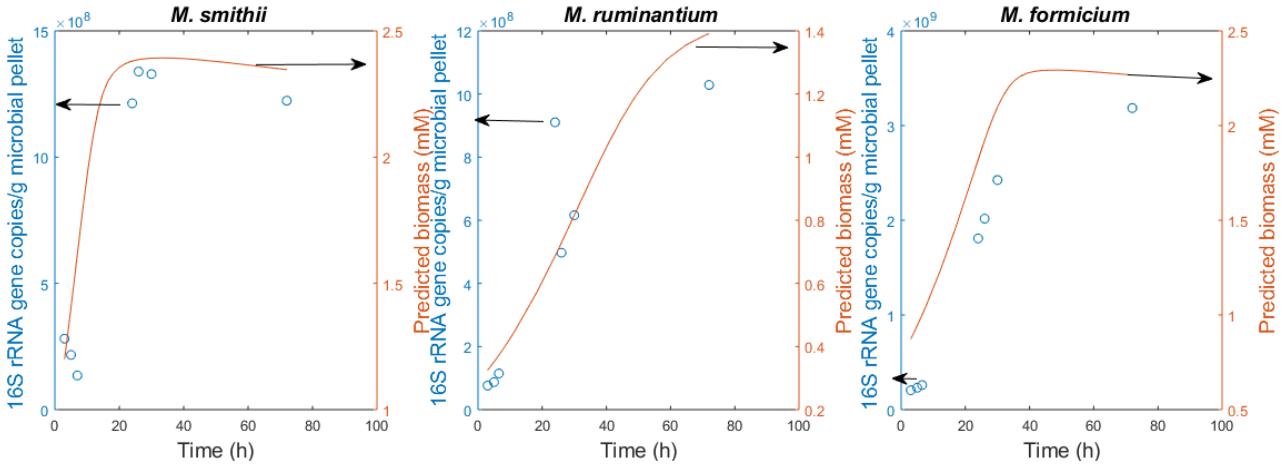

Figure 4 Dynamics of methanogens as measured by 16S rRNA gene copies (circles) and biomass concentrations (solid line) predicted by the model.

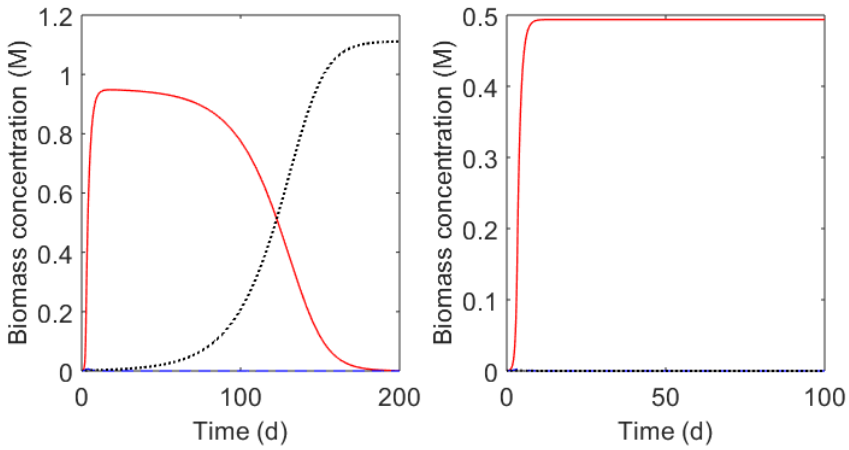

Figure 5 Possible competition scenarios between *M. ruminantium* (blue dashed line), *M. smithii* (red solid line) and *M. formicium* (black dotted line) in a hypothetical constant environment. A. At constant dilution rate of 0.021 h^{-1}, *M. formicium* displaces the other two methanogens. B. With a constant dilution rate of 0.04 h^{-1}, *M. smithii* wins the competition. At constant environmental conditions, only one species wins and displaces the other methanogens.

727

728

729 **Tables**

730 **Table 1** Gibbs energies, enthalpies and entropies of metabolic processes involving some methanogens

731 growing on different energy sources

Microorganism	Energy substrate	Growth conditions	ΔG_m kJ / C-mol	ΔH_m kJ / C-mol	$T\Delta S_m$ kJ / K^{-1} C-mol	Driving force	Reference
M. ruminantium, M. smithii,	H_2/CO_2	anaerobic	-1073	-2132	-1059	Enthalpy-driven but Entropy-retarded	this work
M. formicium	H_2/CO_2	anaerobic	-801	-1605	-804	Enthalpy-driven but Entropy-retarded	this work
M. thermo-autotrophicum	H_2/CO_2	anaerobic	-802	-3730	-2928	Enthalpy-driven but Entropy-retarded	(53)
M. formicium	formate	anaerobic	-880	-613	+267	Enthalpy-driven	(30)
M. barkeri	methanol	anaerobic	-570	-420	+150	Enthalpy-driven	(30)

M. barkeri	acetate	anaerobic	-366	+145	+511	Entropy-driven but enthalpy-retarded	(76)

732 **Table 2** Parameters of the model of *in vitro* methanogenesis. The value reported

733 μ_{max} for each methanogen is the mean value obtained from three heat flux-time curves

Parameter	Definition	Value		
$k_L a$ (h^{-1})	Liquid–gas transfer constant	8.33		
K_{H,CO_2} (M/bar)	Henry's law coefficient of carbon dioxide	0.0246		
k_d (h^{-1})	Death cell rate constant	8.33×10^{-4}		
		M. smithii	*M. ruminantium*	*M. formicium*
K_s (mol/L)	Affinity constant	0.028	0.042	0.011
μ_{max} (h^{-1})	Maximum specific growth rate constant	0.12	0.07	0.046
Y (mol biomass /mol H_2)	Microbial biomass yield factor	0.006	0.006	0.007

734

735 **Table 3** Statistical indicators for model evaluation

Component	CCC^{*}	r^2	$CV_{RMSE}{}^{**}$
Hydrogen	0.99	0.97	14
Methane	0.97	0.95	18
Carbon dioxide	0.94	0.88	6

736 * CCC: Lin's concordance correlation coefficient.

737 ** CV_{RMSE}: coefficient of variation of the root mean squared error.

738

739

740

741

742

743

744

745

746

747

748

749

750

751

Supplementary Material

Hydrogenotrophic methanogens of the mammalian gut: functionally similar, thermodynamically different - A modelling approach

Rafael Muñoz-Tamayo[1*,¶], Milka Popova[2, ¶], Maxence Tillier[2], Diego P. Morgavi [2], Jean-Pierre Morel [3], Gérard Fonty [3], Nicole Morel-Desrosiers[3]

[1]UMR Modélisation Systémique Appliquée aux Ruminants, INRA, AgroParisTech, Université Paris-Saclay, 75005, Paris, France

[2]Institute National de la Recherche Agronomique, UMR1213 Herbivores, Clermont Université, VetAgro Sup, UMR Herbivores, Clermont-Ferrand, France

[3]Université Clermont Auvergne, CNRS, LMGE, F-63000 Clermont-Ferrand, France

1. Growth media information and inoculation conditions

Table S1 Methanogens growth media composition (modified from DSMZ medium 119 https://www.dsmz.de/microorganisms/medium/pdf/DSMZ_Medium119.pdf . Growth media was distributed in Balch tubes (6 ml per tube), tubes were sealed and sterilized by autoclaving at 121°C for 20 min. Media preparation and distribution was realized under CO_2 flushing to assure anoxic conditions. Oxygen traces from commercial gases were scrubbed using a heated cylinder containing reduced copper (35).

Composition per 100 ml	**Amount**
Clarified rumen fluid [1]	30 ml
Dipotassium phosphate (K_2HPO_4) 0.06% (w/v)	5 ml
Balch Mineral solution [3]	5 ml
Tryptone	0.2 g
Yeast extract	0.2 g
Balch oligo-elements solution [4]	1 ml
Balch vitamin solution[5]	1 ml
Resazurin 0.1%[2]	1 ml

Ammonium chloride	0.05 g
Sodium acetate	0.25 g
Sodium formate	0.25 g
Sodium carbonate	0.5g
L-cystein HCl[2]	0.4g
Distilled water	qs 100 ml

[1] Rumen fluid, that was the main constituent of the culture medium, was sampled through the rumen cannula from a grazing dairy cow prior to the beginning of the experiment. Sampled rumen contents were strained through a monofilament cloth, the filtrate was then centrifuged at 5 000 g for 15 min. The supernatant was autoclaved and centrifuged again at the same conditions as above. The clarified rumen fluid (decanted supernatant) was stored at -20°C and centrifuged again after thawing prior to media preparation.

[2] Media was boiled to expel dissolved oxygen, a reducing agent (L-cystein) and a redox indicator (resazurin) were added to keep a low redox potential and indicate the oxidative state of the medium, respectively.

[3] $KH_2PO_4.2H_2O$ (0.6g), $(NH_4)_2SO_4$ (0.6g), NaCl (1.2g), $MgSO_4.7H_2O$ (0.12g), $CaCl_2.2H_2O$ (0.12g), distilled water qs 100 ml

[4] Nitrilotriacetic acid (0.15 g), $MgSO_4.7H_2O$ (0.3g), $MnSO_4.2H_2O$ (0.05g), NaCl (0.1g), $FeSO_4.7H_2O$ (0.01g), $CoSO_4$ (0.01g), $CaCl_2.2H_2O$ (0.01g), $ZnSO_4.2H_2O$ (0.01g), $CuSO_4.5H_2O$ (0.001g), $AlK(SO_4)_2$ (0.001g), H_3BO_3 (0.001g), $NaMoO_4.2H_2O$ (0.001g), $NiCl.6H_2O$ (0.01g), Na_2SeO_3 (0.001g), distilled water qs 100 ml

[5] Biotine (0.2 mg), PABA (0.5 mg), Riboflavine (0.5 mg), Pantothenic acid (0.5 mg), Sodium ascorbate (0.5 mg), Folic acid (0.2 mg), Niacin (0.5 mg), Pyridoxine (0.10 mg), thiamine (0.05 mg), Vitamin B12 0.1mg/ml (0.1 ml), lipoic acid (0.5 mg), Choline chloride (0.5 mg), Inositol (0.5 mg), Nicotinamide (0.5 mg), Pyridoxal (0.5mg), distilled water qs 100 ml

Table S2 Summary of initial OD and pressure measured immediately after primary inoculation. Presented are means (sd) of 31 values per strain.

Strain	*Methanobrevibacter ruminantium*	*Methanobrevibacter smithii*	*Methanobacterium formicium*
Initial OD	0.054 (0.007)	0.099 (0.027)	0.046 (0.01)
Initial pressure (mbar)	2996 (39.956)	2927 (98.985)	2910 (48.883)

2. Quantification of methanogens

Table S3 qPCR quantification of 16S rRNA genes

	Methanobrevibacter smithii						
Time point (hours after inoculation)	3	5	6.5	24	26	30	72
Microbial pellet (g) *	0.204 (±0.007)	0.16 (±0.017)	0.147 (±0.003)	0.194 (±0.002)	0.182 (±0)	0.176 (±0.012)	0.202 (±0.012)
Extracted DNA ng/g of microbial pellet*	9765.5 (±3078)	12695.1 (±838.4)	13752.8 (±2662.3)	41257.4 (±25296.9)	31983.2 (±512.5)	49386.3 (±3956.8)	28943.7 (±7300.7)
Total number of 16S rRNA gene copies in the microbial pellet	$5.62x10^8$	$4.34x10^8$	$2.71x10^8$	$2.43x10^9$	$2.68x10^9$	$2.66x10^9$	$2.45x10^9$
Total number of cells in the microbial pellet **	$2.81x10^8$	$2.17x10^8$	$1.35x10^8$	$1.21x10^9$	$1.34x10^9$	$1.33x10^9$	$1.22x10^9$
	Methanobrevibacter ruminantium						
Time point (hours after inoculation)	3	5	6.5	24	26	30	72
Microbial pellet (g) *	0.148 (±0.048)	0.134 (±0.006)	0.183 (±0.013)	0.161 (±0.006)	0.153 (±0.039)	0.196 (±0.004)	0.164 (±0.023)
Extracted DNA ng/g of	8764.7 (±1345.4)	10864.3 (±1325.5)	7546.3 (±1126.5)	22274.2 (±16)	19412.8 (±4976.2)	16184.1 (±578.6)	23463.5 (±2053.3)

microbial pellet*							
Total number of 16S rRNA gene copies in the microbial pellet	$1.52x10^8$	$1.74x10^8$	$2.29x10^8$	$1.82x10^9$	$9.95x10^8$	$1.23x10^9$	$2.06x10^9$
Total number of cells in the microbial pellet **	$7.62x10^7$	$8.71x10^7$	$1.15x10^8$	$9.10x10^8$	$4.97x10^8$	$6.16x10^8$	$1.03x10^9$
	Methanobacterium formicium						
Time point (hours after inoculation)	3	5	6.5	24	26	30	72
Microbial pellet (g) *	0.13 (±0.017)	0.167 (±0.017)	0.086 (±0.003)	0.15 (±0.064)	0.167 (±0.044)	0.195 (±0.016)	0.153 (±0.052)
Extracted DNA ng/g of microbial pellet*	19517.7 (±3588.2)	13263.9 (±875)	21530.9 (±7188.2)	63810.6 (±28842.7)	52442.7 (±21309.7)	38602.9 (±2761.3)	60968.8 (±28872.4)
Total number of 16S rRNA gene copies in the microbial pellet	$2.05x10^8$	$2.31x10^8$	$2.60x10^8$	$1.81x10^9$	$2.02x10^9$	$2.42x10^9$	$3.19x10^9$
Total number of cells in the microbial pellet	$2.05x10^8$	$2.31x10^8$	$2.60x10^8$	$1.81x10^9$	$2.02x10^9$	$2.42x10^9$	$3.19x10^9$

* Mean and standar deviation of two observations.
** *M. smithii* and *M. ruminantium* possess two copies of 16S rRNA gene in their genomes.

3. Calculation of thermodynamic properties of the methanogenesis

In our model, the methanogenesis is represented macroscopically by one catabolic reaction (R1) for methane production and one anabolic reaction (R2) for microbial formation. We assumed that ammonia is the only nitrogen source for microbial formation. The molecular formula of microbial biomass was assumed to be $C_5H_7O_2N$ (41).

R_1: $4\ H_2 + CO_2 \rightarrow CH_4 + 2\ H_2O$

R_2: $10\ H_2 + 5\ CO_2 + NH_3 \rightarrow C_5H_7O_2N + 8\ H_2O$

The thermodynamic properties associated to the methanogenesis result from the contribution of both catabolic and anabolic reactions.

3.1 Thermodynamic properties of formation used for the calculations

Table S4 Standard enthalpies ($\Delta H_f°$) and Gibbs energies ($\Delta G_f°$) of formation at 25°C of compounds involved in hydrogenotrophic methanogenesis. Values were extracted from Wagman et al. (77), with the exception of the microbial biomass that was calculated from values for *Methanosarcina barkeri* reported by Liu et al. (76)

Compound (phase)	$\Delta H_f°$ (kJ/mol)	$\Delta G_f°$ (kJ/mol)
H_20 (l)	-285.830	-237.129
H_2 (g)	0	0
CO_2 (g)	-393.509	-394.359
CH_4 (g)	-74.81	-50.72
NH_3 (aq)	-80.29	-26.50
$C_5H_7O_2N$	-511.50*	-349.50*

* These values are five times the values reported by Liu et al. (76) since the biomass formula we used has five carbon molecules, while the biomass formula used by Liu et al. has one carbon.

3.2 Enthalpies

The heat produced during methanogenesis results from the contribution of both catabolic and anabolic reactions. So, first, we calculated the standard enthalpies of the catabolic and anabolic reactions using the standard enthalpies of formation given in Table S4 for the different compounds involved in methanogenesis.

The standard enthalpy of the catabolic reaction $\Delta H^\circ_{r,c}$ was calculated as follows

$$\Delta H^\circ_{r,c} = \Delta H^\circ_{f,CH_4} + 2 \cdot \Delta H^\circ_{f,H_2O} - \left(4 \cdot \Delta H^\circ_{f,H_2} + \Delta H^\circ_{f,CO_2}\right) = -252.96 \frac{kJ}{mol}$$

A similar equation was used for the calculation of the standard enthalpy of the anabolic reaction $\Delta H^{\circ}_{r,a}$

$$\Delta H^{\circ}_{r,a} = \Delta H^{\circ}_{f,C_5H_7O_2N} + 8 \cdot \Delta H^{\circ}_{f,H_2O} - \left(10 \cdot \Delta H^{\circ}_{f,H_2} + 5 \cdot \Delta H^{\circ}_{f,CO_2} + \Delta H^{\circ}_{f,NH_3}\right) = -750.31 \frac{\text{kJ}}{\text{mol}}$$

These results are at 25°C since this is the temperature of the standard enthalpies of formation reported in Table S3. A correction could be made to get results at 39°C but the heat capacities reported by Wagman et al. (77) show that the temperature correction can be neglected. Similarly, in the interest of simplicity, we assumed that the effect of pressure is negligible. Next, we considered the fact that the heat of a given reaction can be calculated at any state along the reaction pathway *via* the determination of the reaction coordinate or degree of advancement ε (78). Under our assumptions, the heat produced or consumed by a particular reaction during a given interval can be calculated as follows

$$Q = \int_{\varepsilon_0}^{\varepsilon_{t_f}} \Delta H^{\circ}_{r} \, d\varepsilon$$

For our two reactions, at the instant t we have

$$\varepsilon_c(t) = \frac{n_{H_2}(t) - f \cdot n_{H_{2,0}}}{-4}$$

$$\varepsilon_a(t) = \frac{n_{H_2}(t) - (1-f) \cdot n_{H_{2,0}}}{-10}$$

where $n_{H_2}(t)$ is the number of moles of hydrogen at the instant t, $n_{H_{2,0}}$ is the initial number of moles of hydrogen, and f is the fraction of H_2 used for the catabolic reaction. Our calorimetric experiments started with $n_{H_{2,0}} = 8.83 \cdot 10^{-5}$ mol in all cases. At the final time t_f, all the hydrogen was consumed, so that $n_{H_2}(t_f) = 0$. For *M. smithii* and *M. ruminantium*, the microbial yield factor is Y=0.006 (6) which implies that f =0.94. Accordingly, $\varepsilon_c = 2.075 \cdot 10^{-5}$ mol and $\varepsilon_a = 5.30 \cdot 10^{-7}$ mol. It thus follows that the overall heat produced during the methanogenesis process (Q_m) can be calculated using the following equation

$$Q_m = Q_c + Q_a = \varepsilon_c(t_f) \cdot \Delta H^{\circ}_{r,c} + \varepsilon_a(t_f) \cdot \Delta H^{\circ}_{r,a}$$

where Q_c , Q_a are the heat produced during catabolism and anabolism respectively. The previous equation can also be written as

$$Q_m = n_{H_{2,0}} \left[\frac{(1-10Y)}{4} \, . \, \Delta H^{\circ}_{r,c} + Y \, . \, \Delta H^{\circ}_{r,a}\right]$$

Under the experimental conditions of our study, this yields

$$Q_m = Q_c + Q_a = (-5.25) + (-0.40) = -5.65 \text{ J}$$

This result shows that the anabolic reaction contributes to only 7% of the metabolic heat.

Since the substrate was totally consumed, the enthalpy of the methanogenesis process per mole (or C-mol) of biomass formed, ΔH_{m}, can be calculated as follows

$$\Delta H_{\mathrm{m}} = \frac{Q_{\mathrm{m}}}{n_{\mathrm{biomass}}} = \frac{Q_{\mathrm{m}}}{Y\,.\,n_{\mathrm{H_{2,0}}}} = \frac{(1-10Y)}{4\,.\,Y}\,.\,\Delta H^{\circ}_{\mathrm{r,c}} + \Delta H^{\circ}_{\mathrm{r,a}}$$

which yields

$$\Delta H_{\mathrm{m}} = -10658\frac{\mathrm{kJ}}{\mathrm{mol}} = -2132\frac{\mathrm{kJ}}{\mathrm{C-mol}}$$

For *M. formicium*, Y=0.007 (7). Applying the same procedure, we obtained $Q_{\mathrm{m}} = -5.66$ J and $\Delta H_{\mathrm{m}} = -1830\frac{\mathrm{kJ}}{\mathrm{C-mol}}$

The anabolic reaction contributes to 8% of the metabolic heat.

3.3 Gibbs energies and entropies

Following a procedure analogous to the one used above for the enthalpies, the standard Gibbs energies of the catabolic ($\Delta G^{\circ}_{\mathrm{r,c}}$) and anabolic ($\Delta G^{\circ}_{\mathrm{r,a}}$) reactions were calculated using the standard Gibbs energies of formation listed in Table S3.

$$\Delta G^{\circ}_{\mathrm{r,c}} = \Delta G^{\circ}_{\mathrm{f,CH_4}} + 2\,.\,\Delta \mathrm{G}^{\circ}_{\mathrm{f,H_2O}} - \left(4\,.\,\Delta G^{\circ}_{\mathrm{f,H_2}} + \Delta G^{\circ}_{\mathrm{f,CO_2}}\right) = -130.62\ \frac{\mathrm{kJ}}{\mathrm{mol}}$$

$$\Delta G^{\circ}_{\mathrm{r,a}} = \Delta G^{\circ}_{\mathrm{f,C_5H_2O_7N}} + 8\,.\,\Delta G^{\circ}_{\mathrm{f,H_2O}} - \left(10\,.\,\Delta G^{\circ}_{\mathrm{f,H_2}} + 5\,.\,\Delta G^{\circ}_{\mathrm{f,CO_2}} + \Delta G^{\circ}_{\mathrm{f,NH_3}}\right) = -248.24\,\frac{\mathrm{kJ}}{\mathrm{mol}}$$

The free energy of the methanogenesis process per mole (or C-mol) of biomass formed, ΔG_{m}, can then obtained from the following equation

$$\Delta G_{\mathrm{m}} = \frac{(1-10Y)}{4\,.\,Y}\,.\,\Delta G^{\circ}_{\mathrm{r,c}} + \Delta G^{\circ}_{\mathrm{r,a}}$$

which yields for *M. smithii* and *M. ruminantium*

$$\Delta G_{\mathrm{m}} = -5364\ \frac{\mathrm{kJ}}{\mathrm{mol}} = -1073\ \frac{\mathrm{kJ}}{\mathrm{C-mol}}$$

Knowing that

$$\Delta G_{\mathrm{m}} = \Delta H_{\mathrm{m}} - T.\Delta S_{\mathrm{m}}$$

it follows that the entropic contribution to the methanogenesis process is equal to

$$T.\Delta S_{\mathrm{m}} = \Delta H_{\mathrm{m}} - \Delta G_{\mathrm{m}} = -5294\ \frac{\mathrm{kJ}}{\mathrm{mol}} = -1059\ \frac{\mathrm{kJ}}{\mathrm{C-mol}}$$

which gives, at 39°C, the following value for the entropy of the methanogenesis process per mole (or C-mol) of biomass formed

$$\Delta S_{\mathrm{m}} = \frac{(\Delta H_{\mathrm{m}} - \Delta G_{\mathrm{m}})}{(273.15+39)} = -16.96\ \frac{\mathrm{kJ}}{\mathrm{K\,mol}} = -3.40\ \frac{\mathrm{kJ}}{\mathrm{K\,C-mol}}$$

The same procedure applied to *M. formicium* yields $\Delta G_{\mathrm{m}} = -917\ \frac{\mathrm{kJ}}{\mathrm{C-mol}}, \Delta S_{\mathrm{m}} = -2.92\ \frac{\mathrm{kJ}}{\mathrm{C-mol}}$

References

1. Wolfe RS. Techniques for cultivating methanogens. Methods Enzymol. 2011;494:1–22.

2. Batstone DJ, Keller J, Angelidaki I, Kalyuzhnyi S V, Pavlostathis SG, Rozzi A, et al. Anaerobic Digestion Model No.1 (ADM1). IWA Task Group for Mathematical Modelling of Anaerobic Digestion Processes. IWA Publishing, London; 2002.

3. Wagman DD, Evans WH, Parker VB, Schumm RH, Halow I, Bailey SM, et al. The Nbs Tables of Chemical Thermodynamic Properties - Selected Values for Inorganic and C-1 and C-2 Organic-Substances in Si Units. J Phys Chem Ref Data. 1982;11:S2.

4. Liu JS, Marison IW, von Stockar U. Microbial growth by a net heat up-take: A calorimetric and thermodynamic study on acetotrophic methanogenesis by Methanosarcina barkeri. Biotechnol Bioeng. 2001;75:170–80.

5. Prigogine I, Defay R. Traité de thermodynamique, conformément aux méthodes de Gibbs et De Donder. Éditions Desoer. Liège; 1950.

6. Pavlostathis SG, Miller TL, Wolin MJ. Cellulose Fermentation by Continuous Cultures of Ruminococcus-Albus and Methanobrevibacter-Smithii. Appl Microbiol Biotechnol. 1990;33(1):109–16.

7. Schauer NL, Ferry JG. Metabolism of formate in Methanobacterium formicicum. J Bacteriol. 1980;142:800–7.